JOURNAL OF PROPULSION AND POWER
Vol. 23, No. 4, July–August 2007

Conceptual Design of Americium Nuclear Battery for Space Power Applications

Y. Ronen,* M. Kurtzhand,† L. Droizman,‡ and E. Shwageraus§
Ben-Gurion University of the Negev, 84105 Beer Sheva, Israel

DOI: 10.2514/1.25837

This work presents simplified ^{242m}Am-fueled nuclear battery concept design featuring direct fission products energy conversion and passive heat rejection. Optimization of the battery operating characteristics and dimensions was performed. The calculations of power conversion efficiency under thermal and nuclear design constraints showed that 5.6 W_e/kg power density can be achieved, which corresponds to conversion efficiency of about 4%. A system with about 190 cm outer radius translates into 17.8 MT mass per 100 kW_e. Total power scales linearly with the outer surface area of the battery through which the residual heat is rejected. Tradeoffs between the battery lifetime, mass, dimensions, power rating, and conversion efficiency are presented and discussed. The battery can be used in a wide variety of interplanetary missions with power requirements in the kW to MW range.

Nomenclature

A_i	=	surface area at radius R_i
a	=	fuel layer thickness
E_f	=	recoverable energy per fission
e^+	=	electron charge
f_{esc}	=	FP particle escape probability
I	=	fractional collected current
k	=	thermal conductivity
L	=	FP range
P_e	=	electric power
P_{th}	=	thermal power
Q	=	total fission heat rate
q	=	particle electric charge
T	=	particle kinetic energy
T_i	=	temperature at the radius R_i
U^+	=	applied voltage
$\bar{V}$	=	average FP velocity immediately after escape
V_m/V_f	=	moderator to fuel volume ratio
V_0	=	initial FP velocity
W/gHM	=	watt per gram of initial heavy metal
W_e/kg	=	watt electric per kilogram
x	=	depth at which the fission event occurred
β	=	reduced voltage
μ	=	cosine of the ejection angle
Σ_f	=	fission cross section
σ	=	Stefan–Boltzmann constant
Φ	=	neutron flux

I. Introduction

There is a growing interest [1–3] in nuclear batteries, in particular for space applications. The oldest type of nuclear battery was suggested by Moseley in 1913 (cited in Soo [4]). His device was composed of two electrodes with 150 kV potential and a vacuum between the electrodes; β particles from a radium source of 20 mCi produced a current of 10^{-11} A, leading to a power of 1.5 μW.

The best sources for the direct charging or direct conversion of nuclear batteries [4,5] are the fission products (FP), which have very high energy and carry high electrical charge. A number of experimental and theoretical studies were performed in the past, proving potential feasibility of the direct fission product energy conversion [6,7]. More recently, a comprehensive analysis was performed to explore the direct fission energy conversion options as an alternative to conventional nuclear power reactors [3]. The studies revealed numerous technical challenges associated with the concept. However, two specific design features are of major importance. On one hand, to use the fission products energy directly, the fuel elements must be very thin (on the order of microns), so that the fission products can escape from the fuel. On the other hand, to obtain a critical reactor with high power, conventional nuclear fuels cannot make the reactor critical. The isotope ^{242m}Am has the best nuclear properties with respect to thermal fission. Its thermal cross section is about 7000 barns, which is a factor of 9–10 higher than the cross section of conventional nuclear fuels. Also, the number of prompt neutrons released per fission is relatively high: 3.26 for ^{242m}Am, compared to 2.88 and 2.43 for ^{239}Pu and ^{235}U, respectively. Owing to such superior fissile properties of ^{242m}Am, a critical reactor can be designed with ultrathin fuel elements [8,9].

The half-life of ^{242m}Am is about 141 years, which is sufficiently large for the most practical applications. ^{242m}Am can be obtained by the irradiation of ^{241}Am in a fast neutron spectrum in a nuclear reactor [10,11] and subsequent isotopic enrichment. ^{241}Am, on the other hand, is more readily available, because it is a byproduct of the nuclear fuel cycle in some countries practicing spent fuel reprocessing. ^{241}Am is produced as the result of a β decay of ^{241}Pu with a half-life of 14.4 years.

The battery operates on the principle of direct charging or direct conversion [12], in which the FP kinetic energy is converted directly into electrical energy, using a high voltage potential. The kinetic energy of the FP is thus converted to potential energy and the charges collected in the conductive electrodes create an electrical current.

In this work, we propose a number of improvements to the ^{242m}Am nuclear battery concept initially described in [12]. The objectives of the work are to design a battery with passive cooling and to optimize the battery dimensions and operating conditions to obtain maximum specific electric power from the system: namely, to obtain a system that produces maximum electric power per unit of its mass. In this study, we discuss major tradeoffs between the battery lifetime, mass, dimensions, power rating, and conversion efficiency.

The unique design feature and the major advantage of the improved nuclear battery concept is simplicity. The battery has no moving parts. Therefore, it is inherently more reliable than any nuclear power source with dynamic power conversion. The surface of the battery serves as a radiator to reject the residual

Received 13 June 2006; revision received 31 January 2007; accepted for publication 1 February 2007.

*Department of Nuclear Engineering; yronen@bgu.ac.il.
†Department of Nuclear Engineering; kurtzhan@bgu.ac.il.
‡Department of Nuclear Engineering; droizman@bgu.ac.il.
§Department of Nuclear Engineering; eush@bgu.ac.il.

heat. No active cooling systems are required for the battery operation.

The battery can be used in a wide variety of interplanetary missions with power requirements in the kW to MW range as an alternative to more complex nuclear power systems. The battery can potentially be used to provide electric power to both useful loads onboard of the spacecraft, high I_{SP} thrusters, and, with some modifications, as a power supply on planetary surface.

II. Nuclear Battery Design Description

The conceptual ^{242m}Am nuclear battery design is schematically presented in Fig. 1.

The battery consists of three concentric hollow spheres made of metallic Beryllium. The choice of Be is justified by its good neutron moderation properties, low density, and good electric and thermal conductivities. Both surfaces of the median sphere are plated with metallic ^{242m}Am fuel. This sphere serves as a cathode, emitting positively charged FP towards the inner and outer spheres. The high voltage potential is applied between the median and the two other spheres, creating an electric field that decelerates the FP, so that part of their kinetic energy is converted into electricity.

Here, we present a concept design of the ^{242m}Am-fueled battery with the dimensions and voltage between the electrodes optimized to achieve the highest power conversion efficiency and, as a result, maximum power density of the battery.

III. Evaluation Methodology

Our calculations consist of three major parts: 1) nuclear design, 2) heat removal calculations, and 3) power conversion efficiency calculations.

The total thermal power of the system is determined by the temperature limits on the battery components and its surface area (outer radius). As mentioned earlier, the rest of the battery dimensions and the applied voltage are optimized to achieve maximum electric power density.

The calculations were performed for a set of different battery dimensions and power levels in an iterative manner because nuclear, thermal, and power conversion efficiency calculations are strongly interconnected.

Heat removal is the major design challenge. Therefore, for a given power and battery size, the thermal calculations were performed first with initial guess regarding the inner electrodes dimensions. The total power is adjusted to satisfy the thermal limits. Next, nuclear calculations are performed where electrode thickness (V_m/V_f ratio) is varied to achieve desired criticality. Then, the applied voltage and dimensions of inner electrodes are optimized (conserving the overall V_m/V_f) to achieve maximum power conversion efficiency. Finally, the thermal calculations are performed again to readjust the power to the new battery dimensions and the maximum temperature limit.

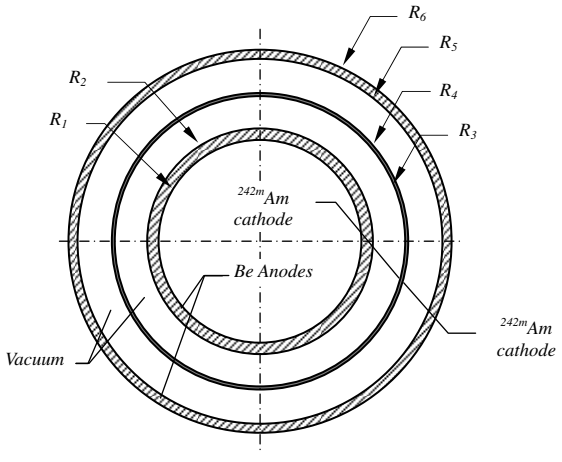

Fig. 1 Nuclear battery geometry.

This procedure is repeated until the system has maximum electric power for a given battery size and satisfies all nuclear and thermal constraints.

A. Nuclear Design

All criticality calculations were performed with MCNP-4C computer code [13] using ENDF-B/VI evaluated cross-section library at room temperature.

In all calculated cases, the criticality of the system was adjusted to k-eff $= 1.06$ by variation of the battery size and Be electrodes thickness. Size of the battery controls the amount of fuel and a leakage of neutrons from the system, whereas thickness of the electrodes controls the moderator to fuel volume ratio (V_m/V_f). An increase in V_m/V_f is generally undesirable because it results in an increase in total mass of the system and corresponding reduction in power density. The size of the battery has an immediate impact heat removal capability because all the waste heat is rejected by radiation through the outer surface.

The value of k-eff $= 1.06$ was chosen because it allows achieving about 20% atomic burnup of the fuel, which is a reasonable assumption from the materials perspective. The achievable burnup estimates were made by reducing the atomic density of ^{242m}Am until k-eff of the system became unity. The reduction in the system criticality is primarily determined by the burnup of ^{242m}Am, because even at 20% atomic burnup, ^{242m}Am is still accounts for most of the neutron absorption (above 99.5%), whereas accumulation of fission products have negligible contribution to overall neutron balance.

Issues related to the battery refueling and reactivity control were not addressed in this work. However, relatively simple refueling options can be considered in the future, which may eliminate the concerns regarding the reactivity limited lifetime of the battery and radiation damage to the cathode. For example, the median sphere plated with Am fuel accounts only for 1–2% of the total battery mass, so that refueling during the mission can definitely be a practical option.

As any power source based on nuclear fission energy, the current battery concept would require radiation shield to protect useful payloads. The shielding design would depend to a great extent on type and duration of the mission, spacecraft design, power level requirements, type of payloads, and more. Because the battery concept presented here is not designed for a specific mission, we did not evaluate the shielding requirements and therefore did not include the shielding mass in our specific power estimates.

B. Power Conversion Efficiency

The energy conversion efficiency is determined by the fraction of fission products that reach the anode and, for those who reach the anode, by the fraction of their remaining kinetic energy. Ideally, the conversion efficiency would be nearly 100% if all fission products will 1) escape the fuel, 2) reach the anode, and 3) have zero kinetic energy at the time of arrival to the anode.

In practice, this is not the case. The FP are born isotropically, so that far less than half of the FP escape the fuel. The rest of the particles either have initial moving direction away from the surface or they are stopped within the fuel layer without escaping. In both cases, all their kinetic energy transforms into direct heating of the cathode sphere.

In the calculations of power conversion efficiency, we made the following additional assumptions:

1) Leakage currents were not taken into account.

2) We assume that all FP have only two distinct kinetic energies (79 and 103 MeV) corresponding to masses of the two most probable ^{242m}Am fission product yields (135 and 103 amu) [14]. This is a reasonable assumption because the main bulk of the fission products have these two atomic masses with standard deviation of about 10%. Therefore, the effect of this assumption on the results of the calculations is expected to be marginal.

3) The emission of fission products is isotropic.

4) Every FP particle striking the emitter is absorbed (no reflection).

5) A large number of low-energy electrons are ejected from the fuel together with the fission products and may significantly impair

the power conversion efficiency. This effect is typically overcome by means of diverting the electrons back to the cathode with relatively weak electric or magnetic field [2,3]. These "insulation" techniques were not considered in the current analysis.

The FP emitted in a direction beyond certain angle relative to the fuel surface will not be collected due to the curvature of the emitting and collecting surfaces as well as nonuniformity of the electric field or the mere fact that the electric field is present. Then, the collected FP particles current I is a function of the applied voltage and geometrical factors. For the outer fuel layer, the collected current is given by [5]

$$I_{\text{outer}}(\beta) = \begin{cases} 1 & \text{if } \beta < 1 - \left(\frac{R_4}{R_5}\right)^2 \\ 1 - \sqrt{1 - \left(\frac{R_5}{R_4}\right)^2 (1-\beta)} & \text{if } \beta > 1 - \left(\frac{R_4}{R_5}\right)^2 \end{cases} \quad (1)$$

where R_4 is the outer radius of the cathode, R_5 is inner radius of the outer anode (Fig. 1), and β is a reduced voltage:

$$\beta = \frac{qU^+}{T} \quad (2)$$

Preliminary assessment showed that optimal distance between the inner fuel layer and inner anode is much smaller than that between the outer fuel layer and the outer anode. Therefore for the inner fuel layer, the collected current was calculated using expression for parallel plates and uniform electric field. In this case, the collected current is given by [5]

$$I_{\text{inner}}(\beta) = (1 - \sqrt{\beta}) \quad (3)$$

The electric power of the system is related to the fission reaction rate as

$$P_e = 2\Sigma_f \Phi V q f_{\text{esc}} I(\beta) U \quad (4)$$

where $2\Sigma_f \Phi V$ is the rate FP particles emission (s^{-1}) and $I(\beta)$ is the total fractional current collected on both outer and inner anodes (dimensionless):

$$I(\beta) = I_{\text{outer}}(\beta) + I_{\text{inner}}(\beta) \quad (5)$$

Finally, the power conversion efficiency of the system is calculated as a ratio of the electric to thermal power:

$$\eta = \frac{P_e}{P_{\dot{m}}} = \frac{2\Sigma_f \Phi V \times 20e^+ \times f_{\text{esc}} \times I(\beta) \times U}{\Sigma_f \Phi V \times E_f} = \frac{20 \times 20e^+ \times f_{\text{esc}} \times I(\beta) \times U}{E_f} \quad (6)$$

where E_f is the recoverable energy per fission for ^{242m}Am ($E_f = 202$ MeV [14]).

The conversion efficiency was optimized to achieve the maximum power density through variation of voltage U, the electrodes dimensions $I(\beta)$, and fuel layer thickness.

C. Consideration of Energy and Charge Losses

Because both electric charge and kinetic energy of the FP are related to the FP's velocity [15,16], we calculated the average velocity of the FP as they leave the fuel layer. The average FP velocity immediately after escape from the fuel layer is given by the following integral relation:

$$\bar{V} = \frac{\int_0^a \int_{x/L}^1 [V_0 - (\mathrm{d}V/\mathrm{d}x)(x/\mu)]\,\mathrm{d}x\,\mathrm{d}\mu}{\int_0^a \int_{x/L}^1 \mathrm{d}x\,\mathrm{d}\mu} \quad (7)$$

In this analysis, we assumed linear velocity loss $\mathrm{d}V/\mathrm{d}x$ to be constant [17] and equal to V_0/L. The FP's range was calculated by SRIM 2003 software [18] and was found to be about 11 μm and 10 μm for the light and heavy FP, respectively.

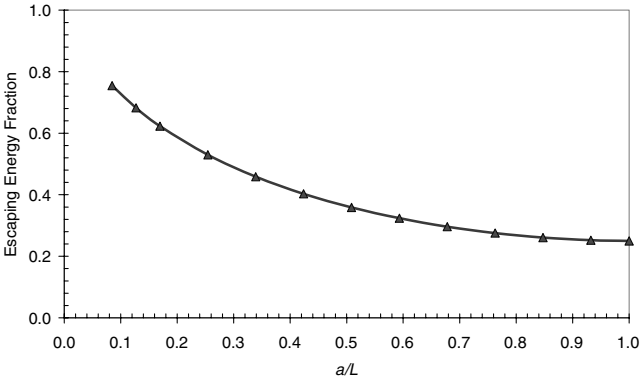

Fig. 2 FP energy fraction escaping from the fuel.

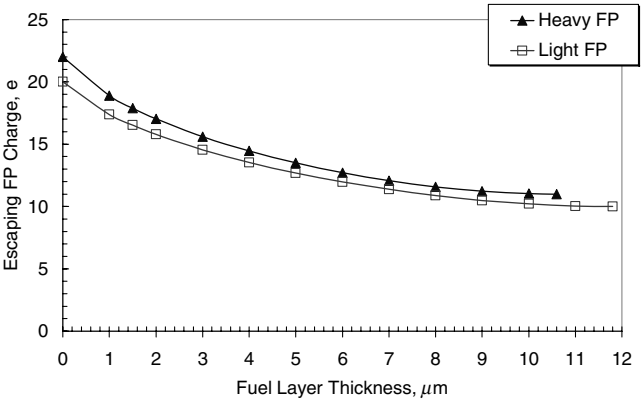

Fig. 3 Average charge of escaping FP.

The FP charge is proportional to the FP velocity [16]. The correlation between the FP energy and the charge according to [16] is

$$\frac{q(E)}{q_0} = \sqrt{\frac{E}{E_0}} = \frac{V}{V_0} \qquad q_0(\text{heavy FP}) = 22\bar{e} \qquad q_0(\text{light FP}) = 20\bar{e} \quad (8)$$

The solution of the integral (7) yields the average FP velocity and therefore the energy fraction and average charge of the escaping FPs. Figures 2 and 3 present the average energy fraction and electric charge of the escaping FP, respectively, as a function of fuel layer thickness. As an example, a fuel thickness of 2 μm allows escaping of about 30% of fission products. The 30% escaping FP fraction is based on the facts that in the isotropic FP emission, only one-half of the FP born in the fuel layer are emitted toward the collected electrode, and for the fuel thickness on the order of 2 μm, only 60% of the fission products energy have a chance to escape (Fig. 2), bringing the overall escaping energy fraction to only 30%.

The thickness of ^{242m}Am fuel layer is a variable parameter affecting power conversion efficiency and battery lifetime. Therefore, it was also a subject for optimization.

Figure 3 shows the loss of FP electric charge as they travel within the fuel layer. As can be observed from the Fig. 3, the average charge of the light and heavy fission products as they escape the 2 μm thick fuel are about $15.5\bar{e}$ and $17\bar{e}$ respectively.

D. Thermal Design

The major thermal design constraint in this analysis is the maximum fuel temperature, which ultimately determines the maximum power for given battery dimensions. The maximum fuel temperature was assumed to be 1076°C, which is about 100°C lower than metallic Am melting point. Operation of the battery at elevated temperatures is challenging from the materials performance perspective, especially in a high-radiation environment. However,

the fact that the battery components carry virtually no mechanical loads somewhat eases these concerns. Changes in electric conductivity of the electrodes with temperature can be neglected because of the relatively large cross-sectional area through which the electric current is collected.

During the battery operation, the heat is transferred by radiation between the electrodes, and by conduction within the electrodes.

Temperature gradient within the fuel layer and thermal contact resistance between the fuel layer and Be electrode were neglected. Emissivity of 100% (black body) was assumed for all battery surfaces.

Heating of the electrodes due to electric current resistance was neglected.

In contrast to electric efficiency calculations, where only kinetic energy of the fission products (182 MeV [14]) was used, all recoverable fission energy (202 MeV [14]) was used in the thermal analysis, which includes energies of all secondary neutron reactions.

We also assumed that both (inner and outer) fuel layers produce the same amount of heat.

The set of equations governing the temperature distribution within the battery components is as follows:

$$\text{Conduction}: \dot{Q} = 4\pi k(T_{i-1} - T_i) \Big/ \left(\frac{1}{R_{i-1}} - \frac{1}{R_i}\right) \tag{9}$$

$$\text{Radiation}: \dot{Q} = A_{i-1}\sigma\left(T_{i-1}^4 - T_i^4\right) \tag{10}$$

where $\sigma = 5.67 \times 10^{-8}\ \text{W/m}^2 \cdot \text{K}^4$, and $k = 190\ \text{W/m} \cdot \text{K}$, the thermal conductivity of beryllium, was assumed to be independent of temperature.

In fact, $\dot{Q}$ should be the total fission heat rate less the power converted into electricity. However, the total fission power was used in thermal calculations to obtain conservative temperature distribution results.

IV. Results and Discussion

A. Optimization of Voltage

Consideration of two (inner and outer) collecting electrodes with different geometries and two distinct energies of the fission products required somewhat detailed analysis to optimize the voltage applied to the electrodes.

In the outer electrode case, for each FP energy, there is a certain voltage limit under which all particles are collected. The greater the particle's kinetic energy, the higher the limiting voltage. For the voltage beyond this limiting value, some part of the FP particles is not collected, but returned to the cathode.

Figure 4 shows the relative fraction of particles collected on the outer electrode as a function of applied voltage for both FP energies as well as the average (between the two energies) collected particles fraction. As can be observed, all particles that escape from the fuel are collected if the voltage is lower than 1.12 MV for the "low-energy" fission product and lower than 1.64 MV for the "high-energy" FP. At

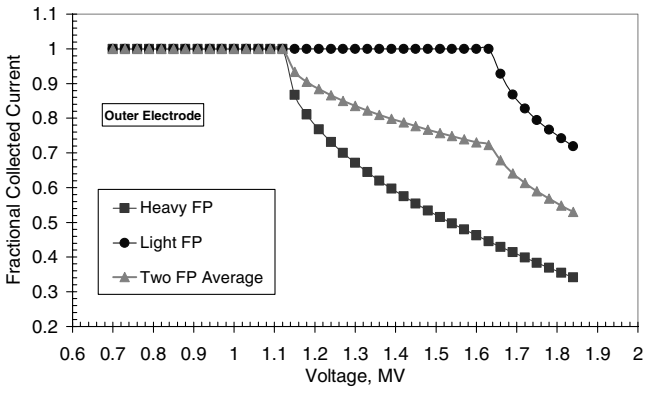

Fig. 4 Fraction of FP collected on the outer electrode.

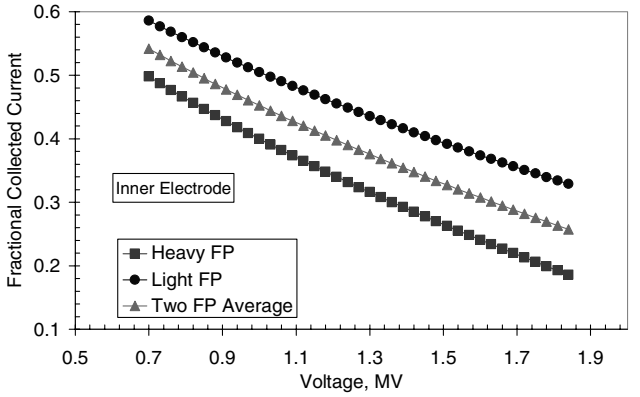

Fig. 5 Fraction of FP collected on the inner electrode.

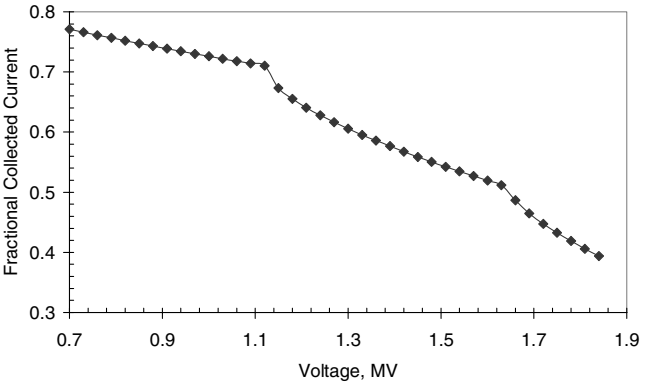

Fig. 6 Fraction of FP collected on both electrodes.

1.64 MV, nearly all high-energy FP are collected, whereas the fraction of collected low-energy FP drops below 50%. On the overall count, over 70% of all FP are collected on the outer electrode at 1.64 MV.

In the inner electrode case, the situation is somewhat different. Under assumption of the parallel plates geometry, all particles are collected only in the absence of electric field. Similar to the outer electrode case, the fraction of collected particles decreases with an increase in the applied voltage (Fig. 5). The efficiency of particles collection is considerably lower for the inner electrode case in comparison with outer electrode case entirely due to geometry effects. For the same voltage range as for the outer electrode case (0.7 to 1.84 MV), the overall fraction of collected particles on the inner electrode is only 55 to 25%.

Figure 6 presents the fraction of the collected particles relative to all FP emitted by both inner and outer fuel layers. The fraction of collected particles decreases monotonically with the voltage from about 75% at 0.7 MV to 40% at 1.84 MV.

The electric power, however, is proportional to the product of voltage and collected particles fraction. As a result, the power increases proportionally to voltage in the voltage region where all particles are collected and decreases sharply with voltage increase in the voltage region where a fraction of the particles is lost. This is illustrated by Fig. 7, which shows the electric power obtained from the outer electrode as a function of the applied voltage for a fixed total battery thermal power of about 2.5 MW_{th}.

In the inner electrode case, the electric power has an optimum (Fig. 8) because the collected particles fraction decreases monotonically with an increase in voltage. In the outer case, the electric power increases proportionally to voltage in the voltage region where all particles are collected and decreases sharply with voltage increase in the voltage region where some fraction of the particles is lost.

Finally, the total electric power is calculated as a sum of the power produced by the FP particles collected on both inner and outer electrodes and presented in Fig. 9. Two peaks observed in Fig. 9

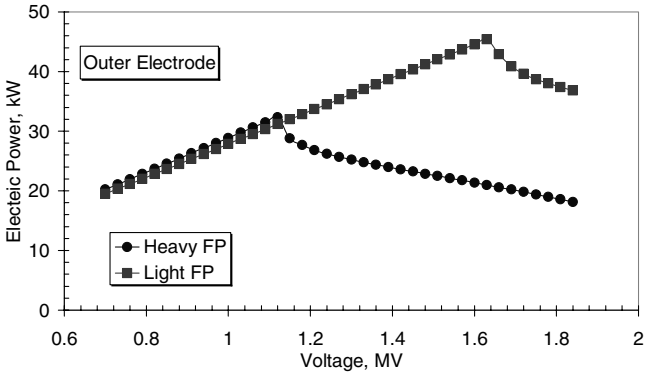

Fig. 7 Electric power obtained from the outer electrode.

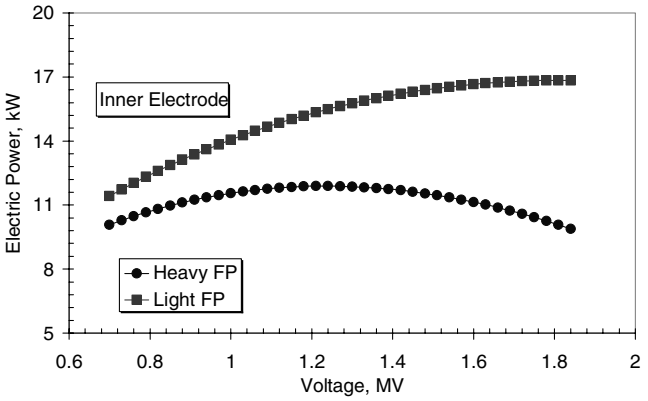

Fig. 8 Electric power obtained from the inner electrode.

correspond to the two FP energies. Adjusting the voltage to the high-FP energy peak is somewhat advantageous because it results in slightly higher (by about 4%) electric power. However, in general, the electric power (or power conversion efficiency) turns out to be relatively insensitive to the applied voltage in the range between 1.1 and 1.64 MV.

The battery produces electric current at comparatively high voltage (on the order of MV). Although dc current is more common in space application, some power conditioning would necessarily be required to connect to useful loads. Because the current battery concept is not designed for a specific application, we did not address any power conditioning issues and did not include power conditioning equipment mass and performance characteristics into the current analysis.

B. Optimization of Electrode Dimensions

The performed analysis showed that the electric power produced by the outer electrode is considerably larger than that produced by the inner electrode. Moreover, the mass of the outer electrode sphere is larger than that of the inner electrode. We found that it is more efficient to adjust the criticality of the system through variation of the outer rather than inner sphere thickness. Therefore, the specific electric power of the battery is more sensitive to the dimensions and power conversion efficiency of the outer electrode than those of the inner electrode. Moreover, the conversion efficiency of the inner electrode favors the minimally possible gap between the electrodes because of the geometry effects. In this work, we assumed 4-cm gap between the inner fuel layer and inner sphere electrode to be a practical guess from the high-voltage engineering considerations taking into account outer space vacuum.

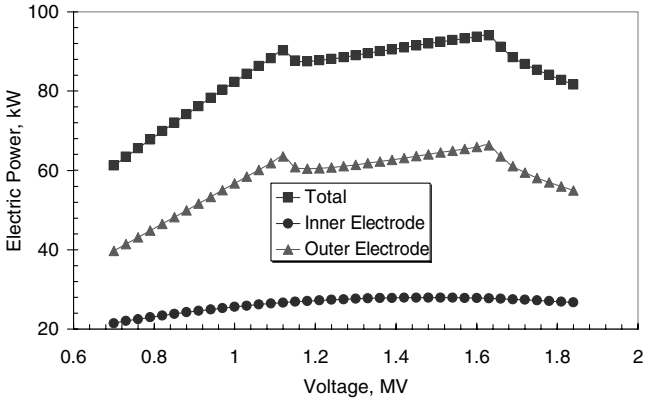

Fig. 9 Total electric power as a function of applied voltage.

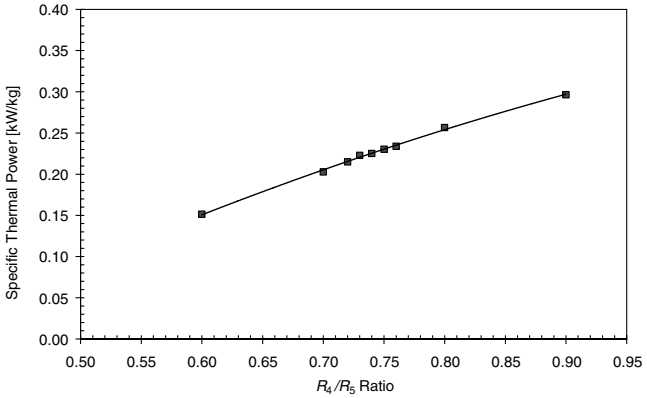

Fig. 10 Specific thermal power dependence on electrode dimensions.

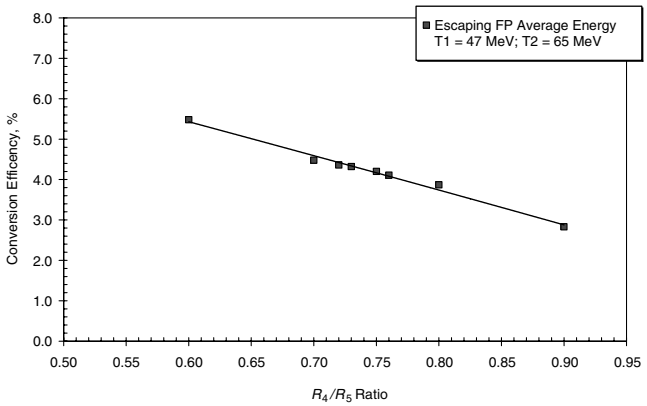

Fig. 11 Power conversion efficiency dependence on electrode dimensions.

The performed analysis showed that for a given battery size and thermal power, the overall conversion efficiency mostly depends on the relative dimensions of the fuel plated sphere (R_4 in Fig. 1) and the outer electrode sphere (R_5 in Fig. 1).

Figures 10 and 11 present the specific thermal power of the battery and the power conversion efficiency, respectively, as a function of R_4/R_5 ratio (Fig. 1). Here, the power conversion efficiency was calculated for a fixed fuel thickness (2 μm) and the dependence of the efficiency on the relative electrode dimensions only was investigated. The optimization of the fuel layer thickness is presented in the subsequent section.

The specific thermal power increases by about a factor of 2 with an increase in R_4/R_5 ratio from 0.6 to 0.9, because both an increase in R_5 and decrease in R_4 lead to an increase in the battery size and mass. The increase in outer surface area results in higher dissipated thermal power, whereas the corresponding increase in the mass is less significant, ultimately resulting in overall increase in the battery power density. On the other hand, the power conversion efficiency decreases by almost a factor of 2 for the same increase in R_4/R_5 ratio.

The opposite trends for the change in specific thermal power and conversion efficiency with R_4/R_5 ratio lead to an existence of an optimum in specific electric power (Fig. 12). If two FP energies are

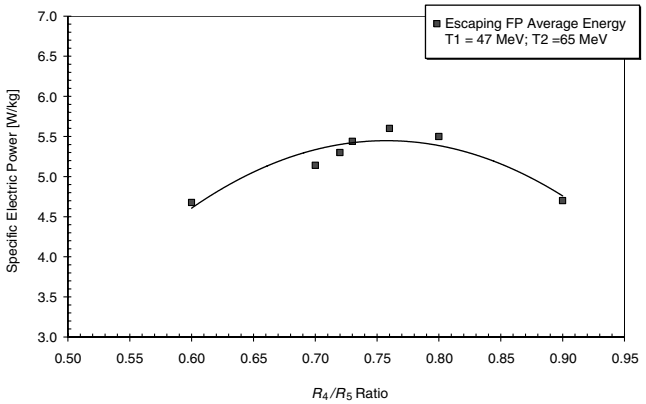

Fig. 12 Specific electric power dependence on electrode dimensions.

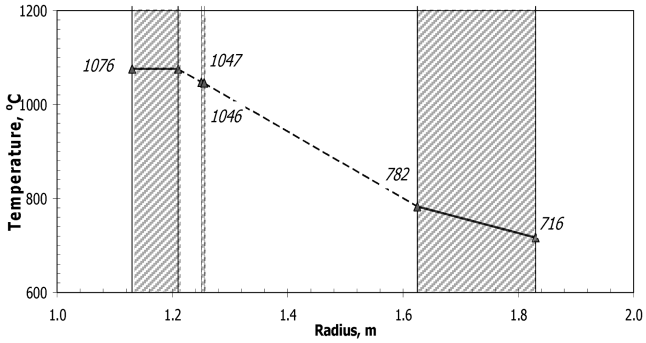

Fig. 13 Battery characteristic temperature distribution.

considered, the optimal specific electric power of 5.6 W/kg is obtained at about $0.76R_4/R_5$ ratio. The corresponding conversion efficiency of this R_4/R_5 value is about 4%.

The temperature field distribution within the battery components is shown in Fig. 13. As can be observed, the maximum temperature of Be does not exceed 1076°C, whereas the maximum fuel temperature is about 1047°C, providing the assumed thermal margin.

C. Optimization of Fuel Thickness

The fuel layer thickness affects several design characteristics. Therefore, it was also subjected to optimization. Thinner fuel would allow higher-energy FP with larger charge to escape the fuel, which would improve power conversion efficiency. On the other hand, to maintain the system criticality, variation of fuel thickness implies either 1) variation in battery dimensions if the fuel mass is to be conserved, or 2) variation in fuel loading if electrodes' dimensions are to be conserved.

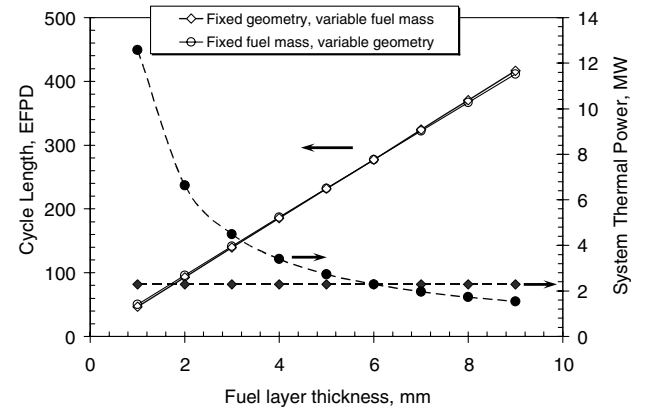

Fig. 14 System thermal power and lifetime.

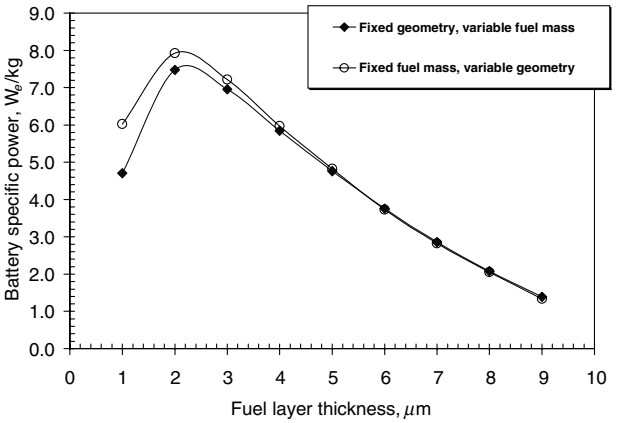

Fig. 15 System specific electric power.

Both cases were investigated, and the results are presented in Figs. 14 and 15. In the first case, for the constant fuel mass, an increase of the fuel thickness results in smaller battery size, therefore lower total power. In the second case, the total power is almost the same because of the same dimensions but reduced fuel loading results in higher W/gHM specific power and reduces the reactivity limited lifetime of the system. In both cases, the changes in criticality are compensated through slight variation of outer electrode thickness and only marginally affect the heat rejection efficiency. The power conversion efficiency is affected only by the fuel layer thickness because ratios between the electrode radii were conserved to maintain the optimal charge collection efficiency reported in the preceding section.

Figure 14 shows linear relation between the fuel mass and reactivity limited lifetime of the system. The linear relation is fairly obvious for the fixed geometry case where less fuel means less energy. This is commonly encountered in commercial reactors where discharge fuel burnup depends linearly of uranium enrichment.

Remarkably, the exact same dependence of the system lifetime on the fuel thickness is observed also for the case where the fuel mass is conserved, which implies that the system power is proportional to the fuel thickness for a given fuel mass. This is explained by the fact that the total power is proportional to the outer surface area, the fuel thickness is proportional to the cathode sphere surface area, and the cathode and outer anode electrode radii are linked through the fixed optimal ratio. Namely, the system power is indeed proportional to the fuel thickness.

For the same reason, the optimal fuel thickness appears to be independent of whether the system geometry or the fuel mass is fixed (Fig. 15). The optimal with respect to the system specific electric power fuel thickness is about 2 μm and represents the tradeoff between the power conversion efficiency, which decreases with fuel thickness, and total mass of the system, which varies due to the nuclear criticality constraint.

Relatively short battery lifetime, on the order of a few hundreds of effective full power days (EFPD), does not necessarily restrict applicability of the concept to comparatively short missions. First, the battery lifetime depends on a number of parameters, which can be traded off with the lifetime. For example, fuel content and moderator to fuel volume ratio can be varied around their optimal values to extend the battery life. In this study, the maximum fuel burnup was chosen somewhat arbitrarily. Innovative fuel forms may permit to achieve higher burnup levels without refueling. Moreover, alternative battery geometry can be considered in the future, which will permit continuous refueling of the battery. In this case, the useful battery lifetime could be extended considerably, extending, in turn, the range of missions to which the nuclear battery concept can be applied.

V. Conclusions

In this work, we proposed a number of improvements to the previously suggested ^{242m}Am nuclear battery concept. The unique

Table 1 Nuclear battery parameters summary

Parameter	Value
Electric power, kW	100
Thermal power, MW	2.3
Conversion efficiency, %	4.0
Battery mass, kg	17,800
Specific electric power, W_e/kg	5.6
^{242m}Am fuel mass, kg	1,072
Outer radius, cm	188
Maximum fuel temperature, °C	1047
Estimated fuel burnup, MWd/kg	175
Estimated lifetime, full power days	80

design feature and major advantage of the improved nuclear battery concept is simplicity. The battery has no moving parts. Therefore, it is inherently more reliable than any nuclear power source with dynamic power conversion. The surface of the battery serves as a radiator to reject the residual heat. No active cooling systems are required for the battery operation.

The main objective of this work was to optimize the battery dimensions and operating conditions to obtain maximum specific electric power. The concept is based on the use of ^{242m}Am as a fuel that makes it possible to design a critical reactor with ultrathin fuel elements: on the order a few μm. Such thin fuel enables the fission products to escape from the fuel and to be used for direct conversion of their kinetic energy into electricity.

The battery consists of three hollow concentric Beryllium spheres. The medial sphere is plated with metallic ^{242m}Am on both sides and serves as a cathode emitting positively charged high-energy fission products. The innermost and the outermost spheres serve as anodes. The thermal power for given battery dimensions is constrained by the maximum fuel temperature, which, in this work, was assumed to be 100 K lower than the melting point of metallic Am. The power scales almost linearly with the surface area of the battery. The system criticality (k-eff = 1.06) represents additional design constraints, which assures about 20% atomic burnup of ^{242m}Am.

Under thermal and nuclear design constraints described in preceding sections, we obtained optimal system components dimensions (ratios between radii of the spheres), applied voltage, and fuel thickness with respect to power conversion efficiency and specific power of the system. The optimal specific electric power is about 5.6 We/kg, which corresponds to about 4% thermal efficiency. The basic parameters of a battery capable of producing 100 kW of electric power are summarized in Table 1. At such a power level, the reactivity limited lifetime (without refueling) of the battery was estimated to be about 80 EFPD.

The system weight and dimensions suggest that applications of the nuclear battery concept is probably impractical for the power levels beyond 1 MW_e where presumably less reliable but much more efficient dynamic power conversion systems become an attractive alternative.

It is important to note, however, that the values for the power density, conversion efficiency, and the battery lifetime are presented only as a reference design point. As stated earlier, these parameters are strongly interconnected and can be altered at the expense of each other. For example, the battery lifetime can be increased through the higher fuel loading and consequently higher fuel thickness, which would ultimately reduce the power conversion efficiency and specific electric power.

The design of the nuclear battery refueling, control, and improvements with respect to fuel compounds with higher meting temperatures will be addressed in the future.

Acknowledgment

The authors would like to acknowledge the help of Gennady Ziskind from the Department of Mechanical Engineering at Ben-Gurion University of the Negev for his suggestions regarding the thermal analysis.

References

[1] Chapline, G., and Matsuda, Y., "Energy Production Using Fission Fragment Rockets," *Fusion Technology*, Vol. 20, Dec. 1991, p. 719.
[2] Tsvetkov, P. V., Hart, R. R., and Parish, T. A., "Highly Efficient Power System Based on Direct Fission Fragment Energy Conversion Utilizing Magnetic Collimation," *Proceedings of the 11th International Conference on Nuclear Engineering, Tokyo, Japan*, ICONE II-36275, 2003.
[3] Slutz, S. A., Seidel, D. B., Lipinski, R. J., Rochau, G. E., and Brown, L. C., "Magnetically Insulated Fission Electric Cells for Direct Energy Conversion," *Physics of Plasmas*, Vol. 10, No. 7, 2003, p. 2983.
[4] Soo, S. L., *Direct Energy Conversion*, Prentice–Hall, Englewood Cliffs, NJ, 1968.
[5] Miley, G. H., *Direct Conversion of Nuclear Radiation Energy*, American Nuclear Society, LaGrange Park, IL, 1970.
[6] Safanov, G., "Direct Conversion of Fission to Electric Energy in Low Temperature Reactors," RAND, Research Report No. RM-1870, 1957.
[7] Krieve, F. W., "JPL Fission-Electric Cell Experiment," JPL, Technical Report No. 32-981, Pasadena, CA, 1966.
[8] Ronen, Y., and Shwageraus, E., "Ultra Thin ^{242m}Am Fuel Elements in Nuclear Reactors," *Nuclear Instruments and Methods in Physics Research A*, Vol. 455, Dec. 2000, pp. 442–451.
[9] Ronen. Y., and Raitses, G., "Ultra Thin ^{242m}Am Fuel Elements in Nuclear Reactors 2," *Nuclear Instruments and Methods in Physics Research A*, Vol. 522, 2004, p. 558.
[10] Kochetkov, A. L., Kazansky, Y. A., Levtchenko, V. A., and Matveenko, L. P., "On Possibility of ^{242m}Am Production in the Special Installations," *Izvestiya Vysshikh Uchebnykh Zavedenii. Yadernaya Energetika*, Vol. 2, No. 2, 2004, p. 52.
[11] Cesana, A., Mongelli, S. T., Terrani, M., Benetti, P., Calligarich, E., Dolfini, R., and Raselli, G. L., "Some Considerations on ^{242m}Am Production in Thermal Reactors," *Nuclear Technology*, Vol. 148, Oct. 2004, p. 97.
[12] Ronen, Y., Hatav, A., and Hazenshprung, N., "^{242m}Am Fueled Nuclear Battery," *Nuclear Instruments and Methods in Physics Research A*, Vol. 531, Oct. 2004, pp. 639–644.
[13] Briesmeister, J. F. (ed.), "MCNP—A General Monte Carlo N-Particle Code, Version 4C," Los Alamos National Laboratory LA-13709-M, Los Alamos, NM, March 2000.
[14] Tsvetkov, P. V., "Direct Fission Fragments Energy Conversion Utilizing Magnetic Collimation," Ph.D. Thesis, Texas A&M Univ., College Station, TX, Dec. 2002.
[15] Bohr, N., "Scattering and Stopping of Fission Fragments," *Physical Review*, Vol. 58, Oct. 1940, pp. 654–655.
[16] Miley, G. H., "Fission Fragment Transport Effects as Related to Fission Electric Cell Efficiencies," *Nuclear Science and Engineering*, Vol. 24, Jan. 1966, pp. 322–331.
[17] Evans, R. D., *The Atomic Nucleus*, McGraw–Hill, New York, 1955.
[18] Ziegler, J. F., "SRIM—The Stopping and Range of Ions in Matter," *Instruction Manual*, IBM Research, Yorktown, NY, Dec. 2005.

G. Spanjers
Associate Editor